

## Article

# Potential Non-Invasive Technique for Accessing Plant Water Contents Using a Radar System

Luís Carlos Santos <sup>1,2,\*</sup> , Filipe Neves dos Santos <sup>1</sup> , Raul Morais <sup>1,2</sup>  and Cândido Duarte <sup>1,3</sup> 

<sup>1</sup> INESC Technology and Science (INESC TEC), 4200-465 Porto, Portugal; filipe.n.santos@inesctec.pt (F.N.d.S.); rmorais@utad.pt (R.M.); candidoduarte@fe.up.pt (C.D.)

<sup>2</sup> Department of Engineering, University of Trás-os-Montes e Alto Douro (UTAD), 5000-801 Vila Real, Portugal

<sup>3</sup> Faculty of Engineering, University of Porto (FEUP), 4200-465 Porto, Portugal

\* Correspondence: luis.c.santos@inesctec.pt

**Abstract:** Sap flow measurements of trees are today the most common method to determine evapotranspiration at the tree and the forest/crop canopy level. They provide independent measurements for flux comparisons and model validation. The most common approach to measure the sap flow is based on intrusive solutions with heaters and thermal sensors. This sap flow sensor technology is not very reliable for more than one season crop; it is intrusive and not adequate for low diameter trunk trees. The non-invasive methods comprise mostly Radio-frequency (RF) technologies, typically using satellite or air-born sources. This system can monitor large fields but cannot measure sap levels of a single plant (precision agriculture). This article studies the hypothesis to use of RF signals attenuation principle to detect variations in the quantity of water present in a single plant. This article presents a well-defined experience to measure water content in leaves, by means of high gains RF antennas, spectrometer, and a robotic arm. Moreover, a similar concept is studied with an off-the-shelf radar solution—for the automotive industry—to detect changes in the water presence in a single plant and leaf. The conclusions indicate a novel potential application of this technology to precision agriculture as the experiments data is directly related to the sap flow variations in plant.

**Keywords:** antennas; precision agriculture; radar; sap flow; water content



**Citation:** Santos, L.C.; dos Santos, F.N.; Morais, R.; Duarte, C. Potential Non-Invasive Technique for Accessing Plant Water Contents Using a Radar System. *Agronomy* **2021**, *11*, 279. <https://doi.org/10.3390/agronomy11020279>

Academic Editor: Heather McNairn

Received: 17 December 2020

Accepted: 28 January 2021

Published: 2 February 2021

**Publisher's Note:** MDPI stays neutral with regard to jurisdictional claims in published maps and institutional affiliations.



**Copyright:** © 2021 by the authors. Licensee MDPI, Basel, Switzerland. This article is an open access article distributed under the terms and conditions of the Creative Commons Attribution (CC BY) license (<https://creativecommons.org/licenses/by/4.0/>).

## 1. Introduction

Agriculture represents an essential sector of the global economy. This activity was adapted along years to fulfil the needs of the world's population, which has duplicated in the last 50 years [1]. Water plays a central role in farming processes and must be tightly controlled to support healthy crops. Precision agriculture and agricultural robotics have been exploiting the potential usage of Variable Rate Technologies (VRT) to control the rate of agronomic inputs, such as water, based on features as plant status and location. Traditional VRT systems consider information from agro-data cloud systems to estimate the correct amount of agronomic inputs. However, these systems do not have access to real-time feedback about the requirements of a plant.

A standard method for water content estimation in individual plants consists of intrusive methods to measure sap flow. There are various types of sap flow measurement based on different principles (e.g., thermodynamic, electric, and magneto-hydrodynamic) with the sensor placed directly into the plant's stem. The most common is the sensor based on thermodynamics, widely used on forest and orchards [2]. These solutions present some drawbacks, as they are invasive, not adequate for plants with thin stems, and not very reliable for more than one season crop.

The non-invasive real-time available solutions comprise mostly radar scatterometers or optical-based systems, typically using satellites or aerial vehicles. These systems can monitor vegetation phenology, including water content of vast planting regions. However,

such approaches cannot measure water content or sap levels at a single or even at individual leaves (i.e., precision agriculture applications). Moreover, satellite radar systems are strongly affected by the interference of other elements, such as soil moisture, terrain topology, cultivation techniques, and atmospheric transmission characteristics [3]. Optical methods can also be used for water sensing by analyzing the reflected electromagnetic signal by vegetation canopies. This reflectance is mostly affected by biological properties, such as the amount of water in the leaves [4]. Nevertheless, the accuracy is negatively affected by atmospheric conditions. Moreover, optical-based methods are limited to superficial layers of plants as only reflected information is used.

The frequency dependency of the water absorption ratio with high radar frequencies (i.e., >8 GHz), provides the best sensitivity on detecting water content in vegetation [5]. This paper presents a device for measuring water content in plants using radiofrequency attenuation for real-time water sensing. This is a previously validated concept that consists of a radio frequency emitter and a receiver, with the element being analyzed in between [6]. This method had demonstrated promising results in the perception of water content of individual leaves. However, it required the development of specific hardware. This work experiments a possible replacement of this hardware by a off-the-shelf ground-based radar solution (EVM AWR1843BOOST). This is a cost-effective and easily available solution. Our goal is to verify its reliability for measure water content/sap flow in plants stems and leaves.

Section 2 presents a bibliographic revision on radar technologies applied to agriculture. Section 3 describes the methodology used for the pre-validated method and the proposed radar approach. Section 4 shows the results of the presented approaches. Section 5 presents the conclusions of this work.

## 2. Related Work

Methods to measure the sap flow in plants have been studied for decades. The most common technique is based on thermodynamics [2], with works retrieving from the 1950s to measure sap flow by heat transport [7]. Typically, these are intrusive sensors composed of needles, like the sensor presented by Vandegehuchte et al. [8]. The authors propose a four-needle method to measure sap flux density and water content, validating the system on stems segments of the European beech tree. Pearsall et al. [9] studied a novel sensor combining heat-pulse and a single set of probes to measure volumetric water user over a range of sap flows in grapevines. Baek et al. [10] monitored water transportation in plant stem with micro-needle sap flow sensor, for fragile hydroponics cultures (i.e., tomatoes and bell peppers). Siqueira et al. [11] presented the Biot-Granier sensor, a strategy to measure sap flow in trees with a new thermal dissipation-based methodology. The sensor was tested with olive trees in a greenhouse, two vineyards and was compared to a commercial solution. The trial with olive trees showed that their sensors showed better results than the commercial one.

Non-invasive techniques for inputs perception in agriculture are mostly based on radar technologies, which have been widely addressed to agriculture purpose for several decades. It is possible to retrieve early works from the 1970s with the application of radar to measure soil moisture content [12]. The radar sensitivity to vegetation originates different volumes of biological matter which affect the wave-plant-soil interaction mechanisms, opening up several possibilities for monitoring crops [13]. Backscatter is the reflection of waves back to the same direction of the transmitted wave. In the application of radar backscatter to agriculture, Susan et al. [14] states that higher frequencies contain more information on vegetation dynamics and lower frequencies minimize the influence of vegetation on backscatter from the soil. Synthetic Aperture Radar (SAR) and Ground Penetrating Radar (GPR) represent two analysis techniques with radar commonly used in agriculture.

SAR is an imaging system that transmits electromagnetic waves with a range of frequencies between 200 MHz to 300 GHz and receives the backscattered signals. The

purpose of SAR is to create an image of the area being analyzed. This radar is typically installed on a moving platform, like aircraft, satellites or truck and tower systems, using the motion to scan a particular place [5,15]. In agriculture, SAR data can be used to analyze soil moisture, crop monitoring and crop classification. Several works use SAR images to infer soil moisture condition, based on the different dielectric constant of soil and water at low frequencies (below 10 GHz) [12,16]. Pascale et al. [17] worked with imaging radars to measure soil moisture until 10 cm of depth, considering a frequency range of 1.5 GHz to 11 GHz from air-borne (AIRSAR) and space-borne (SIR-C) data. Moran et al. [18] investigated the sensitivity of C-Band SAR (5.5 GHz) to surface soil moisture (5 cm depth) in a semiarid range-land with sparse vegetation cover and tested a data fusion approach with optical data (Landsat TM) and radar data (ERS-2 SAR). The study concluded that the sensitivity of the C-Band SAR to soil moisture was relatively low. However, the authors obtained positive results that encouraged the use of multi-temporal SAR and SAR/optical fusion for monitoring semiarid range conditions. Later, MacNairn et al. [19] performed a review about the application of C-band SAR for agriculture with emphasis on RADARSAT-2 system. The authors concluded that radar has a significant advantage over optical sensors because of its weather independence. However, when limited to a single frequency, multi-temporal radar observation will achieve the same level of information as optical sensor that operates in several channels. As well, the capabilities of microwaves with agricultural targets results in a backscatter signal in function of both soil and crop attribute, which complicates the information extraction process. The usage of linear co-polarized or cross-polarized ratios for estimating soil moisture showed good results with vegetation greater than 15 cm tall. Recently, Safa et al. [20] studied the potential of optical and radar Sentinel sensors (Sentinel-1 (S-1) and Sentinel-2 (S-2)) to retrieve soil moisture at regional scale. First, the authors analyzed C-Band radar data from S-1 to measure soil moisture, soil roughness and Leaf Area Index (LAI) over bare soils and cereal fields. Then, the Water Cloud Model was calibrated using the Normalized Difference Vegetation Index (NDVI) retrieved from S-2 images [13].

Remote sensing data from SAR images and scatterometer systems are used to extract useful crop information for monitoring and classification. Burini et al. investigated the sensitivity of backscattering to grape development within space-borne multi-temporal SAR images (ERS2-SAR). They constructed a simple linear model to describe the dependency of the backscattering coefficient on several vegetation variables. The conclusions indicate an increase of backscattering in correspondence of ploughing in March/April, which points out the sensitivity of SAR to some cultivation practices. Moreover, it was noticed an increase of backscattering during summer months, followed by a decrease in the fall, denoting the sensitivity of SAR to the growth of the grapes. Later, Burini et al. [13] performed a multi-temporal L-band SAR (1 GHz to 2 GHz) observation of wine-producing landscape with an air-borne system. These observations were later studied to analyze the sensitivity of L-band SAR to grapes in vineyards, where the results hint at a sensitivity of L-band backscattering to grape biomass per unit area [3]. MacNairn et al.'s [21] research examined a Compact Polarimetric SAR to determine whether SAR data might be used to track crop development similarly to widely adopted optical methods as NDVI. This study used data acquired during six weeks in crops of corn, wheat, and soybeans. The authors found a high coefficient on the correlation between the CP SAR data and the NDVI data for corn and wheat crops. However, the overall coefficient of correlation was 0.56, so, they concluded that further research is merited to integrate SAR-Based index with optical-NDVI. Boryan et al. [22] performed a study to verify the effectiveness of C-band Sentinel-1 SAR data for agricultural flood monitoring. The authors were able to effectively detect and estimate the extent of cropland inundated shortly after Hurricane Harvey in 2017 with 95% accuracy. The study concluded that Sentinel-1 is accurate, affordable, and efficient for this purpose.

So, far, the literature shows that the majority of the radar applications are based on satellite systems. However, for precision agriculture, ground-based approaches can

achieve much higher resolution. Kim et al. [23] resorted to a ground-based multi-frequency scatterometer to evaluate the Radar Vegetation Index (RVI) as a tool to estimate Vegetation Water Content (VWC). The system provides L, C, and X (8 GHz to 12 GHz) bands. The experiment was done in rice fields and soybean crops for approximately 20 weeks. The conclusions indicated backscattering increase in the L-band throughout the growing season and a decrease after harvesting. Martin et al. [24] studied the dielectric response of corn leaves to water stress, as the leaf water content can change during the day, and this affects the radar backscatter significantly. The dielectric response measurements were performed with a micro-strip line resonator with two Teflon blocks placed under and on top of the leaf, with different ranges of frequency, varying between 2 and 4 GHz. The authors concluded that the leaf dielectric properties response to plant growth and water stress depends on the height and age of the leaf. Gao et al. [25] developed a sensor for the detection of the stem water content of woody plants based on standing wave ratio. Windt et al. explored a Nuclear Magnetic Resonance (NMR) to measure the amount of water in living stems of fruits.

To the best of our knowledge, very High-frequency radars (around 80 GHz) were never considered to measure sap flow/water content in plants. Our experiment intends to study the potential of commercial ground-based radar solutions used in the automotive industry to precision agriculture.

### 3. Concept and Methodology

The concept comes from a previously validated method [6], which states that at high frequencies, namely around 20 GHz, the attenuation of a radio-frequency electromagnetic signal is mostly affected by the water content of a plant being irradiated by the beam. This approach was validated with two high gain antennas, an emitter and a receiver, with a leaf between them, as shown in Figure 1.

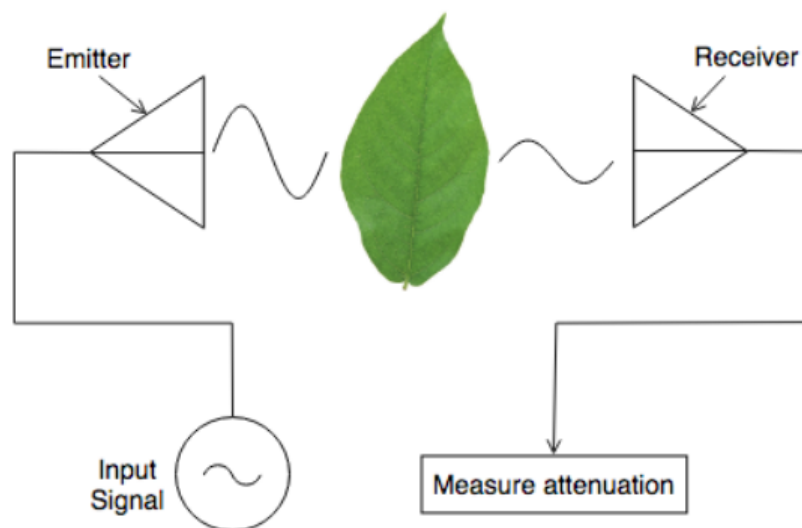
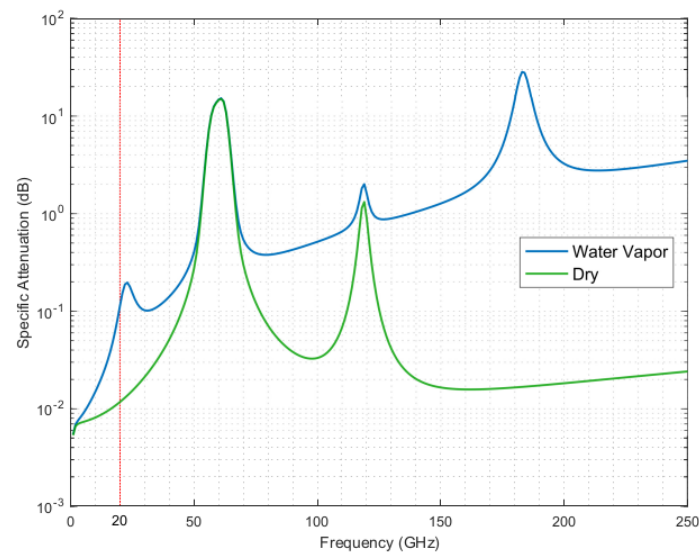


Figure 1. Overview of validated approach [6].

According to Figure 2, there is a peak of attenuation around 20 GHz, and the available equipment maximum frequency was 40 GHz. However, at higher frequencies power loss is even greater.



**Figure 2.** Atmospheric absorption for dry air and air containing water vapor [5].

Given this proven concept, we will apply a similar approach to the commercial radar solution, EVM AWR1843BOOST from Texas Instruments (Figure 3). This evaluation board radar is relatively cost-effective, works at higher frequencies (around 80 GHz), and does not require extra hardware. This board contains a Frequency-Modulated Continuous Wave (FMCW) radar sensor, which works with the reflected signal, expecting the back-scattered wave to suffer attenuation according to the water content present in plants leaves/stems.

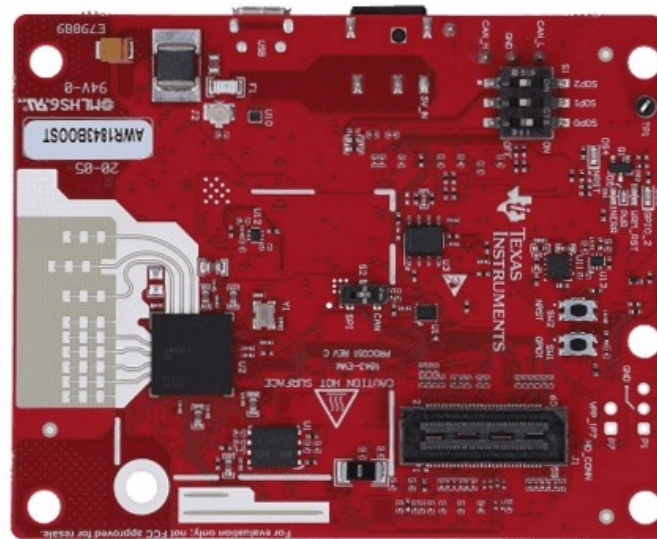


**Figure 3.** EVM AWR1843BOOST from Texas Instruments.

### 3.1. Previous Validation Methodology

The two high gain antennas represented in Figure 1 were placed on a robotic arm, which allowed a high precision scanning of the object to be measured. The pair of antennas were connected to the Vector Network Analyzer (VNA) E8363B PNA Series Network Analyzer (10 MHz to 40 GHz) by KMM24 coaxial cables from Thorlabs. The range of these antennas was between 19.5 GHz and 20.6 GHz, so for all the tests, the measured frequency range was from 19.5 GHz to 20 GHz. Figure 4 shows one of the antennas used during the tests.

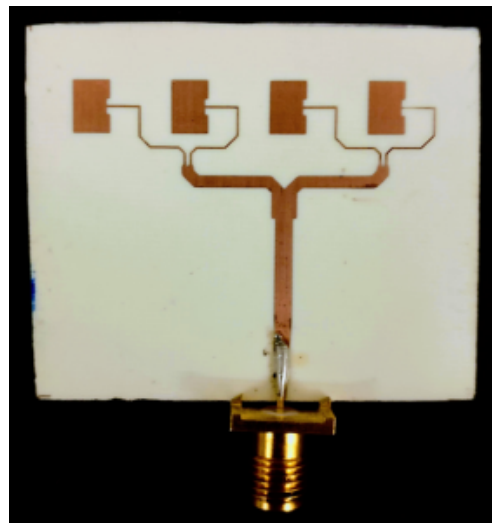


**Figure 4.** High gain antenna used on previous validation tests [5].

For each test, an element was placed between the antenna pair to be scanned. The maximum scanning area was 20 cm by 20 cm, due to physical limitations of the robotic arm. The maximum resolution of the manipulator was 3 mm, which limited the scan step to this value. So, at every scan step, the VNA measured the intensity of the signal transmitted by the emitter antenna on the receiver antenna. Initially, the antennas were placed at a distance of 20 cm, being later positioned at a distance of 9 cm. Figure 5 shows the setup of the antennas without the robotic manipulator used to test sensibility to different water thickness. The antennas installed in the robotic manipulator mounted on top of a robotic platform are represented in Figure 6.

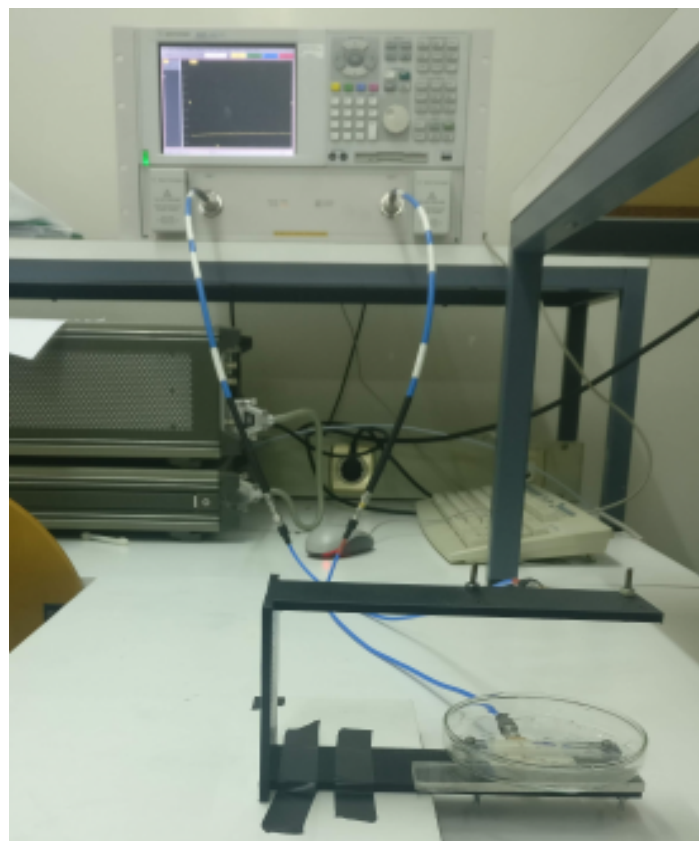


**Figure 5.** Previous Antennas setup to test sensibility to different amounts of water [5].

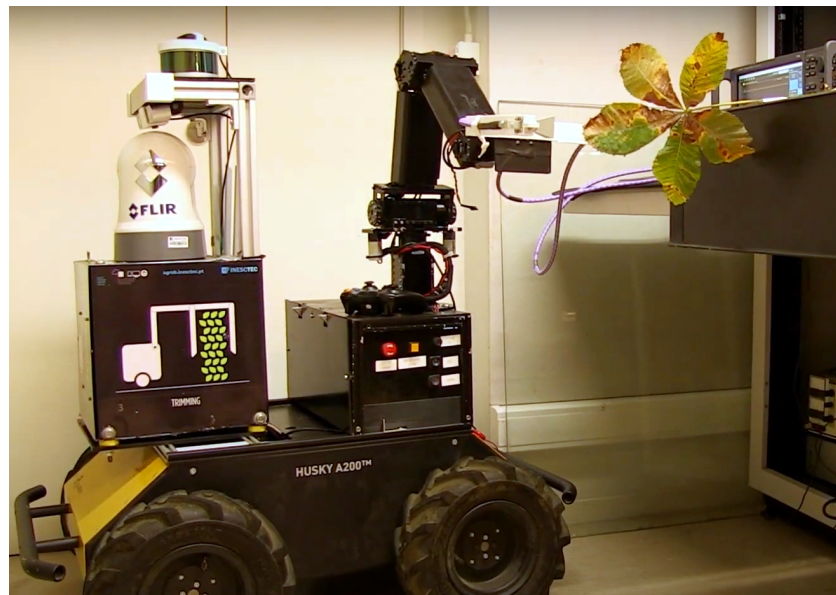


**Figure 6.** Previous Antennas setup with robotic manipulator.

### 3.2. Commercial Radar Methodology

The Evaluation board EVM AWR1843BOOST from Texas Instruments contains seven antennas, where four are receivers, and three are emitters. The board communicates via serial port and can be powered by a simple 5V USB port. So, it only requires a computer compatible with serial communication. The antenna peak gain is  $>10.5$  dBi across the frequency band of 76 to 81 GHz. There are some configurable parameters expressed in Table 1.

**Table 1.** Radar EVM AWR1843BOOST configurable parameters.

Configurable Parameter	Range
Frequency Band (GHz)	76–77 or 77–81
Frame Rate (fps)	1–30
Range Resolution (cm)	3.9–4.7
Maximum Range (m)	3.95–25.21
Maximum Radial Velocity (m/s)	0.32–4.34
Radial Velocity Resolution (m/s)	0.07 or 0.13

Texas Instruments offers a tool, “mmWave Demo Visualizer” [26], for the radar configuration and data visualization. The main plots available are: a scatter plot, a Doppler-range plot, and a range profile for zero Doppler plot. The focus was in the range profile plot, which indicates the power of the signal according to the distance (range). However, this tool only allows to record data in a binary format, which has to be decoded later, without the help of any official tool. Although we managed to decode the information correctly, this operation is time-consuming, as the decoding takes at least the same time as the recording data. So, we used a Robot Operating System (ROS) driver publicly available, “TI mmWave ROS Package” [27]. The recording and manipulation of information are way simpler with ROS, and enables a possible future integration with robotic systems. This ROS driver was not completed by the original authors, leaving some functions not implemented, as the extraction of a range profile plot. So, we wrote the missing code and have performed a request to the original authors to merge their software implementation.

For most of the performed tests, default values from the manufacturer were the main choice:

- 4 receivers antennas and 3 emitters (4Rx,3Tx),
- beam width of  $15^\circ$ ,

- frequency band from 77 GHz to 81 GHz,
- frame rate of 20 fps,
- range resolution of 4.4 cm,
- maximum range of 9.02 m,
- maximum radio velocity of 1 m/s, and
- radial velocity resolution of 0.13 m/s.

Here, the only non-default setting was the frame rate, which was changed from 10 fps to 20 fps to increase the precision in the detection of possible water content.

An aluminium case was placed around the radar antennas to concentrate the signal and increase the sensitivity of the back-scatter to water content. The first test consisted of the validation of the concept that this radar is sensitive to moisture present in plants. So, Figure 7 shows a picture of a white piece of paper sprayed with water in front of the radar.

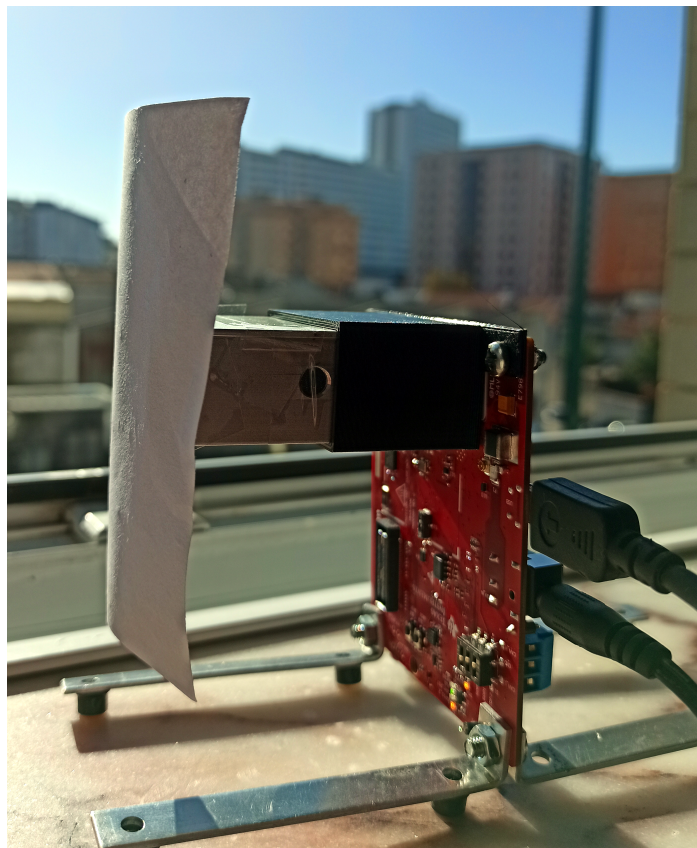


Figure 7. Radar setup to test sensibility to water.

To perform the remaining tests, the radar antennas were headed to a plant's leaf or stem. Two types of tests were considered: one approach consisted of collecting data for several hours. In the other method, while recording data from the radar, the plant was placed in a zone with direct solar exposition. Then, after a few minutes, we block the sunlight and remove this block after some time. The goal is to force a variation in the sap flow of the plant and verify the radar's sensitivity to this change. The tests were performed on a kale's stem and an Orchid leaf, as shown in Figure 8.



**Figure 8.** Radar setup to performs tests with a kale’s stem (**left**) and an orchid leaf (**right**).

#### 4. Results

This section presents the experimental results obtained in the previous validation experiments (for patent publication) with the two high-gain antennas, and the results obtained with the radar AWR1843BOOST. All the times indicated during the tests are according to Greenwich Mean Time Zone (GMT). The sunrise/sunset schedules were confirmed with the 2020 calendar available in the Aeronautical Information Service (AIS) from NAV Portugal [28].

##### 4.1. Previous Validated Method Results

This method used a robotic arm to perform a scan. So, the result is a greyscale image containing information about the intensity of the received signal. So, white pixels represent the lowest intensity (more significant attenuation), and black pixels represent the highest intensity (lowest attenuation) [6]. For the tests represented below, black pixel means 0 dB attenuation, and white pixels means 6.59 dB attenuation [5].

The following tests consisted of a scan of a cactus-like plant, in Figure 9; a half-brown leaf, in Figure 10; and a leaf before and after drying, in Figure 11.

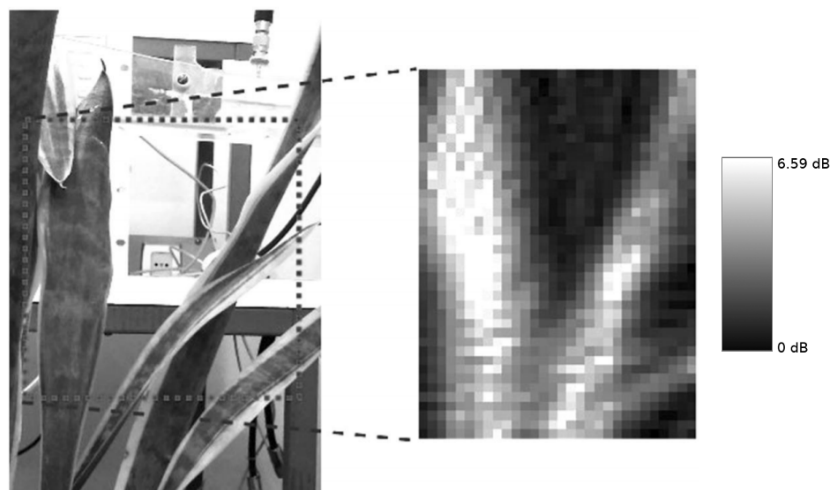


**Figure 9.** Test results with a cactus-like plant [6].

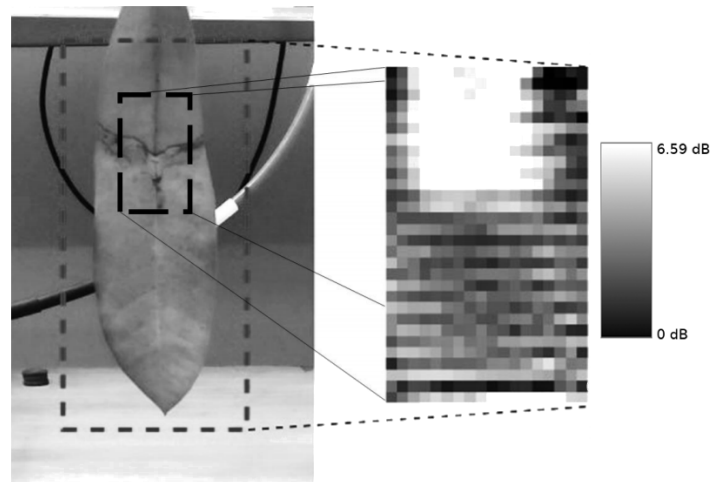


Figure 10. Test results with a half-brown leaf [6].

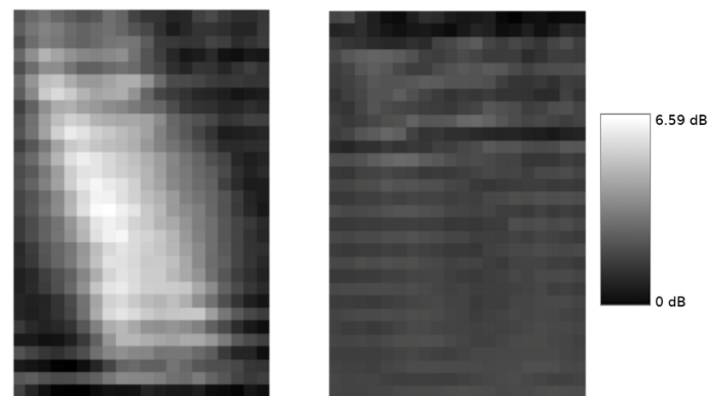


Figure 11. Test results with a green leaf (left) and dry leaf (right) [6].

#### 4.2. Results with Radar EVM AWR1843BOOST

Here, all the tests were static, and no scans were performed. The results can be demonstrated with: a plot of various signals of range profile data, a plot of a specific component of all range profile signals varying with time, or both plots.

##### 4.2.1. Test with Water Sprayed on a Piece of Paper

The first test was performed with a white piece of paper sprayed with water in a zone with direct sunlight exposure. The setup was presented in Figure 7, and the results are represented in Figure 12. This figure shows a plot with 20 range profile signals. Each signal represents the average of the 1200 frames emitted per minute (20 fps). The figure also shows the temporal evolution corresponding to a specific  $range = 5$ , chosen for being the most variable component of the signals. Both graphics clearly demonstrate a decrease in the signal intensity over time. The intensity keeps decreasing in the first 10 min and stabilizes from here. This is expected, as a piece of paper sprayed with water will undoubtedly dry after 10 min of solar exposure. So, it is observable that the signal's intensity is directly related to the water content.

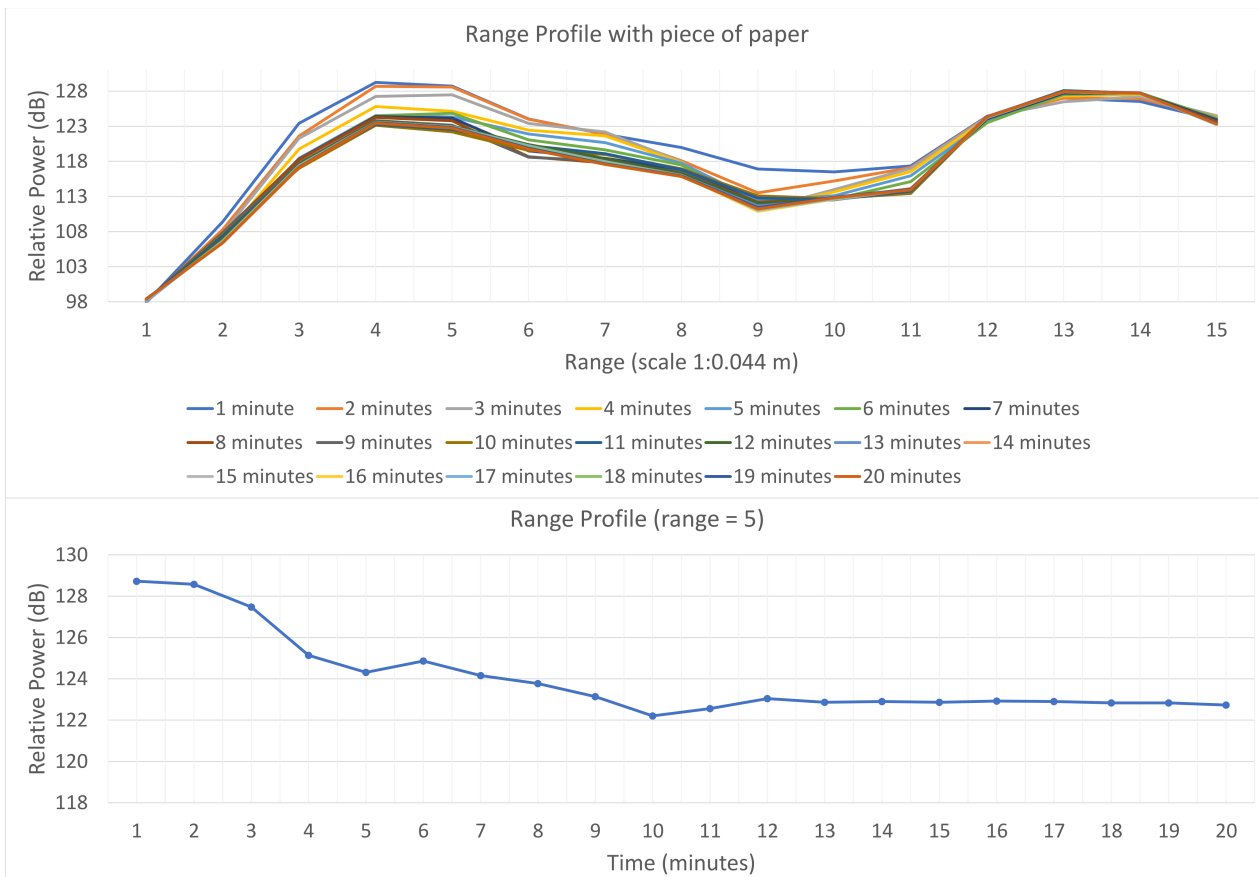


**Figure 12.** Test results with a sprayed piece of paper.

#### 4.2.2. Test with Orchid Leaf

This test consisted of collecting data from the radar for 40 min with the setup depicted in Figure 8 and took place in the city of Porto, Portugal, on 17 November 2020 at 9:50 in the morning. On this day, the sunrise had occurred at 07:26.

The orchid was in a place with direct sun exposure for 10 min. Then, we blocked the sunlight for 10 min, removed the block after other 10 min, and finally blocked the solar exposition for the remaining time. This experiment is illustrated in Figure 13, where red lines represent the block or unblock of solar exposition and the periods with sun exposition are represented by a symbol of the sun in the left corner. The results indicate an apparent attenuation of the signal at the 10th minute, followed by a small increase at the 20th minute. At the 30th, the range profile suffers another attenuation peak, maintaining stability until the end of the test. With this experiment, the plant's photosynthesis was interrupted for specific periods of time, causing variations in the sap flow. The reaction seems to be almost immediate when the sunlight gets blocked. This is expected as the sap flow from the roots to the leaves is interrupted. However, when the block is removed, the expected increase in the signal's intensity is not so powerful. In order to stabilize the values, we may have to extend the duration of sun exposure.

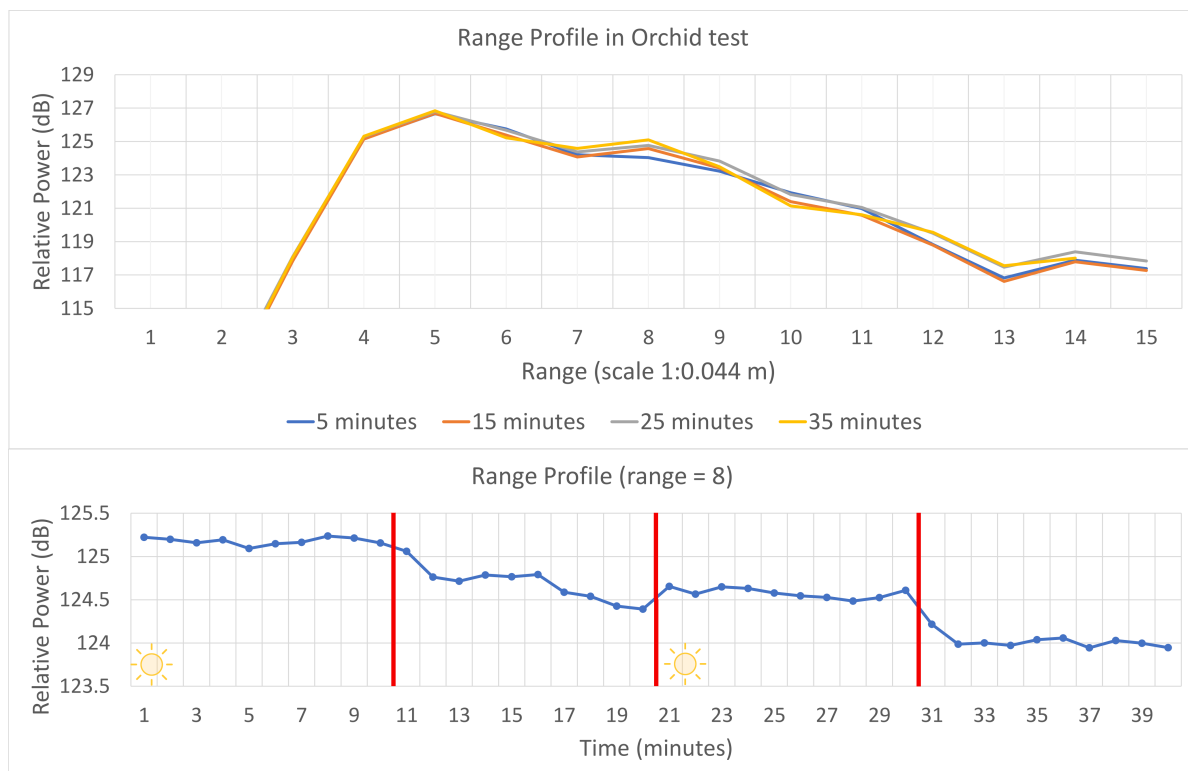


**Figure 13.** Test results with an orchid; red lines—block or unblock of solar exposition.

#### 4.2.3. Test with Kale's Stem

Two tests took place with the radar pointed to a kale's stem, as shown in Figure 8.

The first test was similar to the orchid test, with the results presented in Figure 14. Similarly to the orchid, the kale was directly exposed to the sun and while blocking and unblocking the sunlight. These blocks are represented with a red line, and the symbol of the sun indicates solar exposition during that time interval. Here, the intervals are not constant, and at the minute 85, the plant was watered.

The test took place in the city of Porto, Portugal, on 19 November 2020, at 10:35 in the morning. The duration was of 105 min. On this day, the sunrise had occurred at 07:28.

The range profile plot (Figure 14) indicates a slight increase in the intensity during the first 15 min without direct sunlight exposure. We can also observe a small rise of the power by the 15th minute and a rising peak around the 22nd minute. This could be justified by a more substantial sunlight exposure at this hour of the day. The signal tends to stabilize after 30 min when the sunlight is blocked. Then, there is an upward trend from the 46th minute. There is a sign of stabilization again by the minute 65, without direct sunlight, and another small rise by the 76th minute. By minute 85, the kale was watered, which caused an increase. Then, the signal kept stable until the end of the test.

The second test consisted of collecting data for several hours during day/night and night/day transition. This test also took place in the city of Porto, on 19 November 2020, and start at 02:10 in the afternoon. The sunset occurred at 05:10. The duration of the test was of 350 min (6 h).

The plots with the results are designed in Figure 15. The top plot shows the average of the range profile signal until the minute 180 and the average from this minute until the end of the test. The bottom plot focuses on the time variation of one specific range. There is a power decrease along the afternoon, with an abrupt fall around the 180th minute. This corresponds to 05:10 in the afternoon, which coincides with the sunset. From here, the signal does not suffer relevant variations until the end of the test.

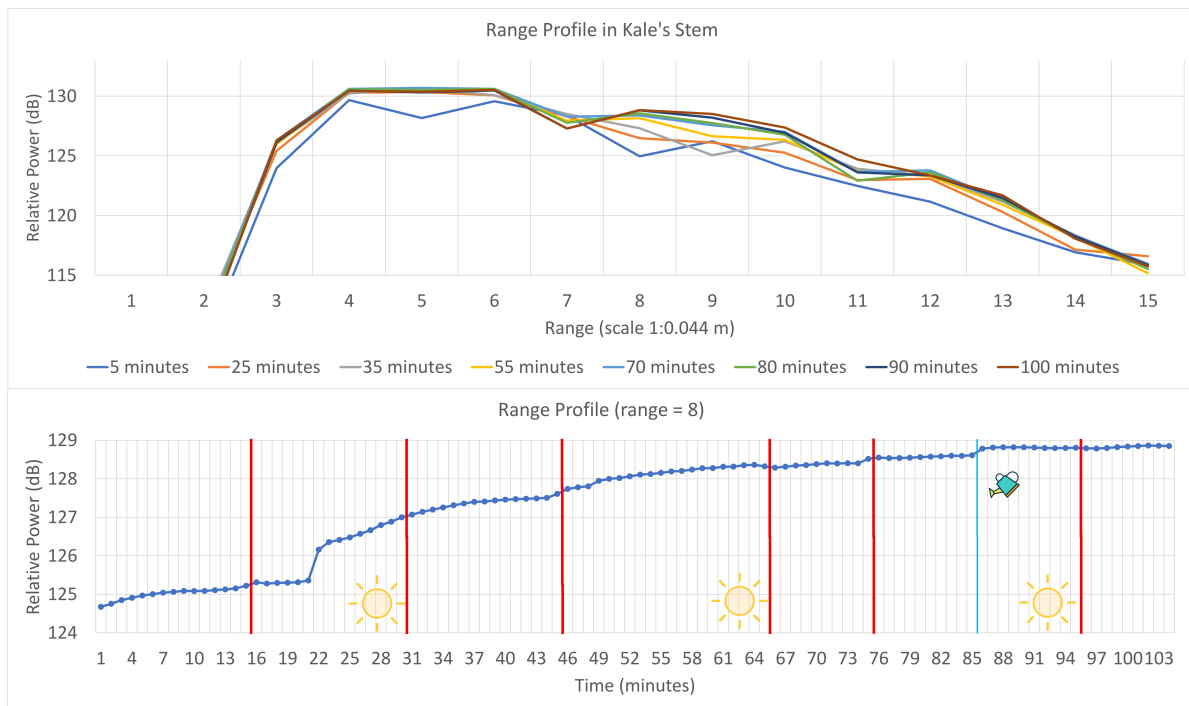


Figure 14. Result of the first test with kale’s stem; red lines—block or unblock of solar exposition; vertical blue line—watering.

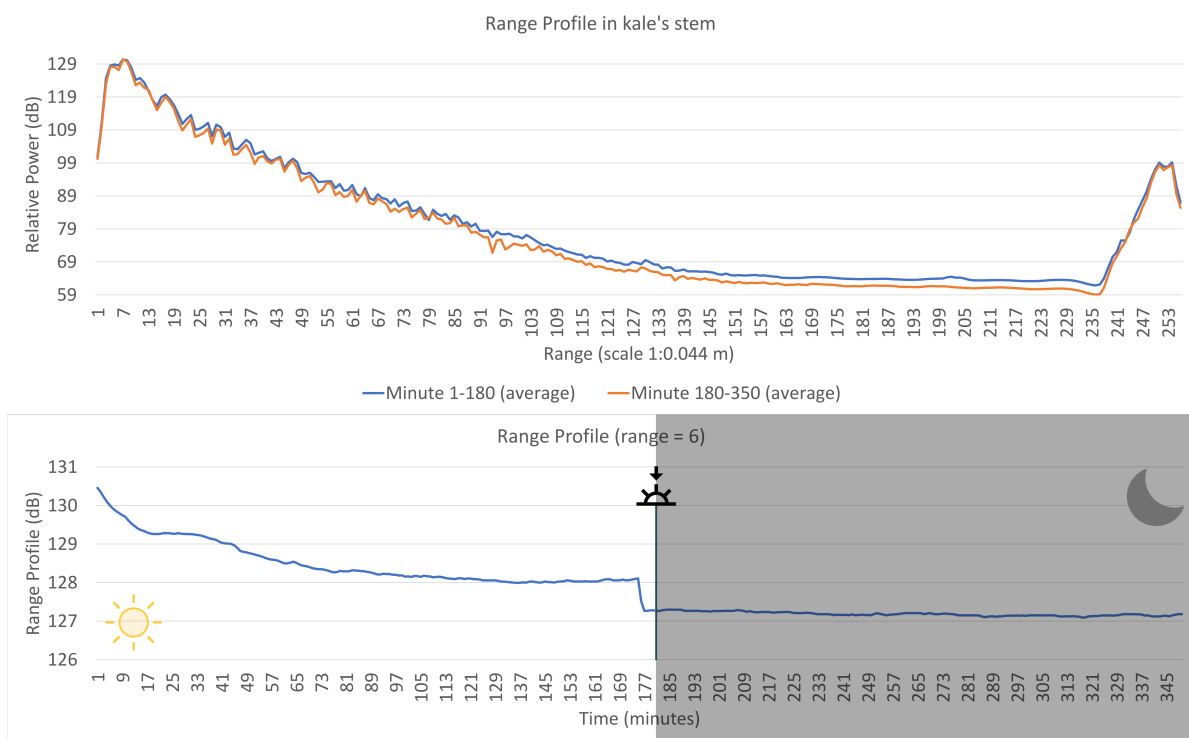
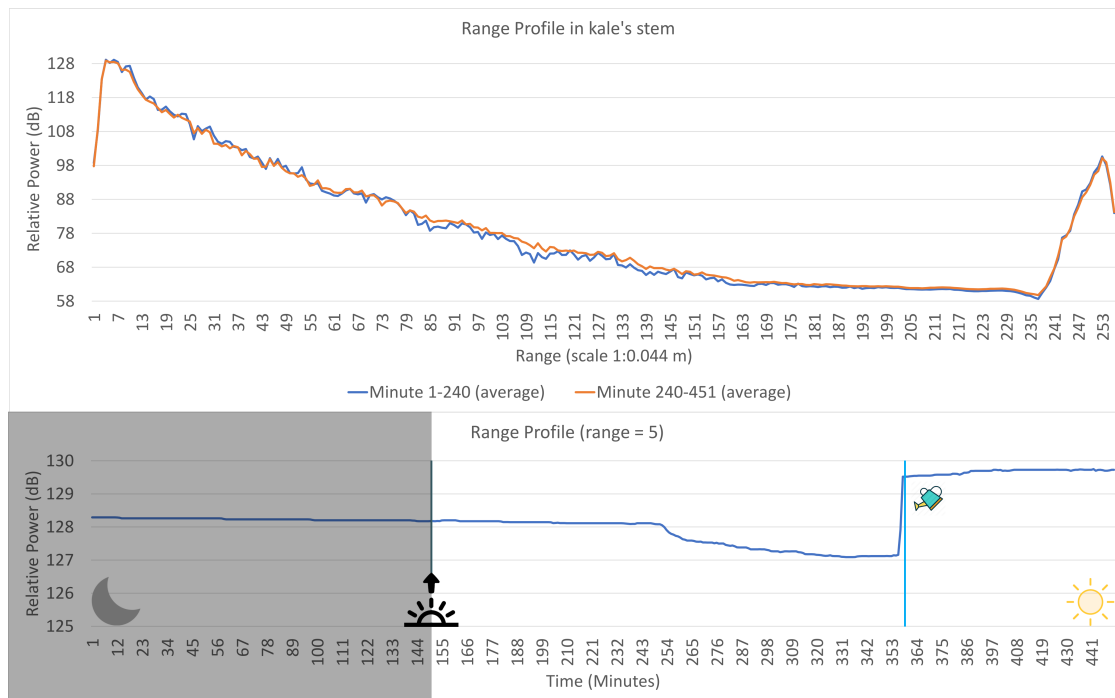


Figure 15. Result of the second test with kale’s stem during the day/night transition; vertical line: sunset.

Then, the same test was performed during the night/day transition. This test started on 20 November 2020, at 5:00 in the morning, with a duration of 451 min (8 h). The sunrise occurred at 07:29.

The plots with the results are designed in Figure 16. The top plot shows the average of the range profile signal until the minute 240, and the average from this minute until the end of the test. The bottom plot focuses on the time variation of one specific range. The signals intensity is stable with a slight decrease during the night time, but, after the sunrise,

there were no observed changes in this pattern. This could be justified with the lack of direct sunlight for the next two hours. However, the signal's intensity fall accentuated two hours after the sunrise and continued to descend until the 360th minute. Here, we considered that the kale was with water stress, and watered it. As visible in the plot, the power increased immediately, stabilizing with a slight increase until the end of the test.



**Figure 16.** Result of the second test with kale's stem during the night/day transition; vertical black line: sunrise; vertical blue line: watering.

## 5. Conclusions

The current paper presented a non-invasive method to detect water content present in plants. The first method presented here was previously validated [6]. It places an element (leaf) in between two high gain antennas and measures the signal's attenuation caused by the water content in the element. This system resorts to a robotic arm to scan the entire leaf and create a grey level image according to the signal attenuation. So, the whiter this image, the more water content is present in the element. This method required the use of coaxial cables and a VNA machine which was limited to a maximum of 40 GHz frequencies.

The second method consisted of the study of the commercial radar solution, EVM AWR1843BOOST from Texas Instruments, to detect variations in the water content/sap flow in plants. This solution works with frequencies around 80 GHz and only requires a regular computer for setup and data collection. We modified a non-official python script to decoded data recorded with the official tool of Texas Instruments, which was not compatible with our board. However, we performed all tests using an ROS driver, that was modified, as well in order to process information about the radar range profile (not implemented by the original developer). The performed tests showed a direct relation of the range profile data with the water content. During the test with a water sprayed piece of paper, the signal's relative power decreased as the paper sheet dried. In the tests with plants (kale and orchid), we started by forcing variation in the sap flow by intermittently blocking the sunlight, and verified a decrease in the intensity of the signal when the plant did not have direct solar exposition. On the other hand, the power tended to increase with direct sun exposure. The plant was watered in one of the experiments, which caused a rise in the signal's power. The findings indicate a more expressive variation with the kale, which is expected as orchids are plants known for their low water consumption.

When measuring during long periods of time, it was observed that, along an afternoon, the radar signal's power decreases as solar exposition reduces. This fall is more abrupt around sunset. In our last experiment, a negative variation in the range profile relative power was detected after sunrise. This was an indicator of water stress, as the values suffered an abrupt rise after watering.

This phenomena, which also occurred when the kale was watered during the tests with intermittent sunlight blocks, proves that the changes in the signal occur due to variations in water content and not other factors, like possible variations of temperature.

To conclude, this commercial solution has a potential application for precision agriculture purposes, namely measuring variations in water content or sap flow in individual plants. With the results of this work, we can clearly associate variation in the signal's intensity with sap flow changes. Positive variation indicates an increase of the water content, while negative variation points out the opposite. The greater the variation, the bigger the change in the sap flow. Nevertheless, at this stage, it is not possible to quantify water levels present in plants yet, as our data consistency is on the intensity variation and not precisely its value.

As future work, we will realize more measuring tests with other plants/trees (e.g., vine trees), and modify radar parameters, like resolution, antennas configuration, and maximum range. The variation will be mathematically associated with a specific amount of water content, and the radar module will be integrated with an embedded system (e.g., raspberry pi). Alternative and traditional methods may be considered to measure ground-truth values. Additional boards may be used to enable additional functionality. For example, DCA1000EVM from Texas Instruments enables access to the sensor's raw data, which could improve our results. There is even the possibility of modifying the hardware in order to change the antennas localization. With this, we could place the plant in between the antennas, and the system would be more similar to the previously validated method. Notwithstanding, this would not be a direct application of a commercial solution.

## 6. Patents

Method and Device for Measuring Water Present in Vegetation [6].

**Author Contributions:** Conceptualization, F.N.d.S. and C.D.; methodology, F.N.d.S., C.D., L.C.S., and R.M.; software, L.C.S.; validation, F.N.d.S., L.C.S., and C.D.; formal analysis, F.N.d.S., R.M., C.D., and L.C.S.; investigation, L.C.S.; resources, F.N.d.S.; data curation, F.N.d.S. and L.C.S.; writing—original draft preparation, L.C.S.; writing—review and editing, F.N.d.S., R.M., and C.D.; visualization, F.N.d.S., R.M., and C.D.; supervision, F.N.d.S. and R.M.; project administration, F.N.d.S.; funding acquisition, F.N.d.S. All authors have read and agreed to the published version of the manuscript.

**Funding:** This work is financed by National Funds through the Portuguese funding agency, FCT—Fundação para a Ciência e a Tecnologia within project UIDB/50014/2020, and project “Water-JPI/0012/2016”. The authors would like to thank the EU and FCT for funding in the frame of the collaborative international consortium Water4Ever financed under the ERA-NET Water Works 2015 cofounded call. This ERA-NET is an integral part of the 2016 Joint Activities developed by the Water Challenge for a changing world joint programme initiation (Water JPI).

**Institutional Review Board Statement:** Not applicable.

**Informed Consent Statement:** Not applicable.

**Conflicts of Interest:** The authors declare no conflict of interest.

## References

1. Kitzes, J.; Wackernagel, M.; Loh, J.; Peller, A.; Goldfinger, S.; Cheng, D.; Tea, K. Shrink and share: Humanity's present and future Ecological Footprint. *Philos. Trans. R. Soc. B Biol. Sci.* **2007**, *363*, 467–475. [[CrossRef](#)] [[PubMed](#)]
2. Čermák, J.; Kučera, J.; Nadezhdina, N. Sap flow measurements with some thermodynamic methods, flow integration within trees and scaling up from sample trees to entire forest stands. *Trees* **2004**, *18*, 529–546. [[CrossRef](#)]

3. Schiavon, G.; Solimini, D.; Burini, A. Sensitivity of multi-temporal high resolution polarimetric C and L-band SAR to grapes in vineyards. In Proceedings of the 2007 IEEE International Geoscience and Remote Sensing Symposium, Barcelona, Spain, 23–27 July 2007; pp. 3651–3654.
4. Hunt, E.R., Jr.; Rock, B.N. Detection of changes in leaf water content using near-and middle-infrared reflectances. *Remote Sens. Environ.* **1989**, *30*, 43–54.
5. Borges, R.G. *Noninvasive Techniques for Vine Perception*; Faculty of Engineering of the University of Porto, Porto, Portugal, 2018.
6. Dos Santos, C.M.; dos Santos, F.B.; Gomes, R.B. Method and Device for Measuring Water Present in Vegetation. 2020. Available online: <https://worldwide.espacenet.com/patent/search/family/066001101/publication/EP3674703A1?q=pn%3DEP3674703A1%3F> (accessed on 1 February 2021).
7. Marshall, D. Measurement of sap flow in conifers by heat transport. *Plant Physiol.* **1958**, *33*, 385. [[CrossRef](#)] [[PubMed](#)]
8. Vandegheuchte, M.W.; Steppe, K. Sapflow+: A four-needle heat-pulse sap flow sensor enabling nonempirical sap flux density and water content measurements. *New Phytol.* **2012**, *196*, 306–317. [[CrossRef](#)] [[PubMed](#)]
9. Pearsall, K.R.; Williams, L.E.; Castorani, S.; Bleby, T.M.; McElrone, A.J. Evaluating the potential of a novel dual heat-pulse sensor to measure volumetric water use in grapevines under a range of flow conditions. *Funct. Plant Biol.* **2014**, *41*, 874–883. [[CrossRef](#)] [[PubMed](#)]
10. Baek, S.; Jeon, E.; Park, K.S.; Yeo, K.H.; Lee, J. Monitoring of water transportation in plant stem with microneedle sap flow sensor. *J. Microelectromech. Syst.* **2018**, *27*, 440–447. [[CrossRef](#)]
11. Siqueira, J.M.; Paço, T.A.; Machado da Silva, J.; Silvestre, J.C. Biot-Granier Sensor: A Novel Strategy to Measuring Sap Flow in Trees. *Sensors* **2020**, *20*, 3538. [[CrossRef](#)] [[PubMed](#)]
12. Ulaby, F. Radar measurement of soil moisture content. *IEEE Trans. Antennas Propag.* **1974**, *22*, 257–265. [[CrossRef](#)]
13. Burini, A.; Del Frate, F.; Minchella, A.; Schiavon, G.; Solimini, D.; Bianchi, R.; Fusco, L.; Horn, R. Multi-temporal High-resolution Polarimetric L-band SAR Observation of a Wine-producing Landscape. In Proceedings of the 2006 IEEE International Symposium on Geoscience and Remote Sensing, Denver, CO, USA, 31 July–4 August 2006; pp. 501–503.
14. Steele-Dunne, S.C.; McNairn, H.; Monsivais-Huertero, A.; Judge, J.; Liu, P.W.; Papathanassiou, K. Radar remote sensing of agricultural canopies: A review. *IEEE J. Sel. Top. Appl. Earth Obs. Remote Sens.* **2017**, *10*, 2249–2273. [[CrossRef](#)]
15. Moreira, A.; Prats-Iraola, P.; Younis, M.; Krieger, G.; Hajnsek, I.; Papathanassiou, K. A tutorial on synthetic aperture radar. *IEEE Geosci. Remote Sens. Mag.* **2013**, *1*, 6–43. [[CrossRef](#)]
16. Ulaby, F.T.; Dubois, P.C.; Van Zyl, J. Radar mapping of surface soil moisture. *J. Hydrol.* **1996**, *184*, 57–84. [[CrossRef](#)]
17. Dubois, P.C.; van Zyl, J.; Engman, T. Measuring soil moisture with imaging radars. *IEEE Trans. Geosci. Remote Sens.* **1995**, *33*, 915–926. [[CrossRef](#)]
18. Moran, M.S.; Hymer, D.C.; Qi, J.; Sano, E.E. Soil moisture evaluation using multi-temporal synthetic aperture radar (SAR) in semiarid rangeland. *Agric. For. Meteorol.* **2000**, *105*, 69–80. [[CrossRef](#)]
19. McNairn, H.; Brisco, B. The application of C-band polarimetric SAR for agriculture: A review. *Can. J. Remote Sens.* **2004**, *30*, 525–542. [[CrossRef](#)]
20. Bousbih, S.; Zribi, M.; Mougenot, B.; Fanise, P.; Lili-Chabaane, Z.; Baghdadi, N. Monitoring of surface soil moisture based on optical and radar data over agricultural fields. In Proceedings of the 2018 4th International Conference on Advanced Technologies for Signal and Image Processing (ATSIP), Sousse, Tunisia, 21–24 March 2018; pp. 1–5.
21. McNairn, H.; Homayouni, S.; Hosseini, M.; Powers, J.; Beckett, K.; Parkinson, W. Compact polarimetric synthetic aperture radar for monitoring crop condition. In Proceedings of the 2017 IEEE International Geoscience and Remote Sensing Symposium (IGARSS), Fort Worth, TX, USA, 23–28 July 2017; pp. 4358–4361.
22. Boryan, C.G.; Yang, Z.; Sandborn, A.; Willis, P.; Haack, B. Operational Agricultural Flood Monitoring with Sentinel-1 Synthetic Aperture Radar. In Proceedings of the IGARSS 2018-2018 IEEE International Geoscience and Remote Sensing Symposium, Valencia, Spain, 22–27 July 2018; pp. 5831–5834.
23. Kim, Y.; Jackson, T.; Bindlish, R.; Lee, H.; Hong, S. Radar vegetation index for estimating the vegetation water content of rice and soybean. *IEEE Geosci. Remote Sens. Lett.* **2011**, *9*, 564–568.
24. Van Emmerik, T.; Steele-Dunne, S.C.; Judge, J.; Van De Giesen, N. Dielectric response of corn leaves to water stress. *IEEE Geosci. Remote Sens. Lett.* **2016**, *14*, 8–12. [[CrossRef](#)]
25. Gao, C.; Zhao, Y.; Zhao, Y. A novel sensor for noninvasive detection of in situ stem water content based on standing wave ratio. *J. Sens.* **2019**, 2019. [[CrossRef](#)]
26. mmWave Demo Visualizer. 2020. Available online: [https://dev.ti.com/gallery/view/mmwave/mmWave\\_Demo\\_Visualizer/ver/3.5.0/](https://dev.ti.com/gallery/view/mmwave/mmWave_Demo_Visualizer/ver/3.5.0/) (accessed on 20 November 2020).
27. TI mmWave ROS Package. 2020. Available online: [https://github.com/radar-lab/ti\\_mmwave\\_ropkg](https://github.com/radar-lab/ti_mmwave_ropkg) (accessed on 20 November 2020).
28. SunSise/SunSet Tables. 2020. Available online: <https://www.nav.pt/en/ais/sunrise-sunset-tables> (accessed on 20 November 2020).